Biochemical Engineering Journal 205 (2024) 109249

Contents lists available at ScienceDirect

Biochemical Engineering Journal

journal homepage: www.elsevier.com/locate/bej

Regular article

Renewable gases production coupled to synthetic wastewater treatment through a microbial electrolysis cell

Lorenzo Cristiani [1], Marco Zeppilli [*], Giuliano Fazi, Clara Marandola, Marianna Villano

Department of Chemistry University of Rome Sapienza, P.Le Aldo Moro 5, Rome 00185, Italy

ARTICLE INFO

Keywords:
Biogas Upgrading
Microbial electrolysis cell
Bioelectromethanogenesis
Green hydrogen
Hythane

ABSTRACT

This study describes the use of a microbial electrolysis cells for the production of gaseous biofuels sustained by the oxidation of a synthetic wastewater. During the overall experimental investigation, the MEC's bioanode removed on average 855 ± 57 mgCOD/d producing an average electric current of 66 ± 7 mA which was diverted into gaseous biofuels like biomethane, biohydrogen and biohythane. Three different MEC cathodic configurations were investigated selecting the electrodic materials (graphite granules GG, and mixed metal oxide MMO) and operating conditions (pH of the catholyte, additional sorption chamber). Biomethane production increased from 26 ± 4–102 ± 8 meq/d when the MMO electrode was used with respect to GG electrodic material. In contrast, the MMO electrode in combination with a CO_2 sorption chamber was successfully utilized for simultaneous H_2 production and CO_2 sorption from a N_2/CO_2 mixture which simulates an anaerobic digestion biogas. The combination of H_2 production and CO_2 sorption allowed to obtain a gaseous mixture composed of 9% H_2, 5% CO_2, and 80% N_2 that according to the assumption of replacing the N_2/CO_2 mixture with real biogas corresponded to a commercial-grade biohythane. Overall, the results highlight the potential of MECs as an efficient approach for biogas upgrading, allowing biohythane production increasing CH_4 content and lowering CO_2 concentration.

1. Introduction

Biogas, produced through anaerobic digestion (AD), consists of a gas mixture mainly composed by methane (50–70%, v/v) and carbon dioxide (30–50%, v/v) [1]. Other impurities such as NH_3 and H_2S are presented in small amount (0–300 ppm and 50–5000 ppm respectively) [2]. The specific biogas composition depends on the selected substrate and reactor set-up. Biogas applications are limited due to its low calorific value, which is caused by the low ratio of CH_4/CO_2 [3]. To obtain biomethane, whose characteristics are similar to compressed natural gas (CNG) (with a concentration of CH_4 > 95% v/v), purification and upgrading steps are required to remove impurities (e.g., NH_3 and H_2S) and CO_2, respectively [4]. These steps are typically based on physiochemical methods such as water scrubbing, pressure swing adsorption and membrane separation that are energy- consuming and economically expensive [5], features that do not match the current problems related to pollution and high-cost energy demand [6,7]. In this context, microbial electrolysis cells (MECs) represent a cost-effective and environmental-friendly alternative to physicochemical technique for upgrading biogas [8,9]. MECs are an innovative strategy for biological biogas upgrading in which bio-electroactive microorganisms carry out the reduction of CO_2 to CH_4 by using a cathode as electrons donor [10,11], while the electroactive oxidation of organic matter in the bioanode partially sustains the energy demand of the process [12]. In contrast with physiochemical methods according to which CO_2 is removed from the gas mixture relying on its physical-chemical properties, in biological upgrading the bioconversion of CO_2 into CH_4 is performed [13]. This is perfectly in line with EU guidelines for GHGs emission reduction and renewable energy production [14], moreover, the recent REPowerEU Plan [15] establishes that 35 billion cubic meters (bcm)/year of the 155 bcm/year currently imported natural gas, should be replaced by domestic biomethane production by 2030. Considering that 1 ton (i.e. 1.53 billion m^3) of biogas can produce approximately 2 tons (i.e. 1.01 billion m^3) of biogenic CO_2 during the biogas upgrading process, by 2030, the EU area could generate 42 Mton/year of biogenic CO_2, making the potential of the sectors of carbon capture, storage and utilization very

* Corresponding author.
E-mail address: marco.zeppilli@uniroma1.it (M. Zeppilli).
[1] Current address: Department of Bio Pilot Plant, Leibniz Institute for Natural Product Research and Infection Biology - Hans-Knöll Institute, Adolf-Reichwein-Str. 23 07745 Jena, Germany

https://doi.org/10.1016/j.bej.2024.109249
Received 18 December 2023; Received in revised form 3 February 2024; Accepted 4 February 2024
Available online 12 February 2024

significant [16]. The bioconversion of CO_2 to CH_4, called chemoautotrophic biogas upgrading method, is carried out by hydrogenophilic methanogens, players of the last step of anaerobic digestion [17]. To make this process environmentally and economically feasible, H_2 supply must derive from renewable source, so the surplus of renewable electricity derived from solar, or wind power can be used to hydrolyze water for production of H_2 [9]. In this context the coupling of AD and bioelectrochemical systems (BES) is getting more and more attention [18–22]. Indeed, H_2 supply to methanogens represents the limiting step of the process because of the low hydrogen solubility in the liquid phase [23]. Microbial Electrolysis Cells (MECs), a particular type of BES, represents an innovative strategy to overcome this problem, indeed the digestate derived from AD can be directed towards the anodic chamber of a MEC where the oxidation of organic matter, applying an external potential, occurs and it partially sustains the energy demand for CH_4 production supplying the reducing power "in situ" to the methanogenic biofilm growing on the electrode's surface in the cathodic chamber [24, 25]. In this way biogas derived from AD can be addressed to the biocathode with the result of a biogas enriched in CH_4 [26–28]. Moreover, the phenomenon of pH split that occurs at the cathode [29,30], allows the removal of 9 moles of CO_2 for each mole of CH_4 leading to a further increment in terms of methane content [31]. In this study, three different cathodic configurations of a two-chamber filter-press MEC have been investigated for the production of different gaseous biofuels (i.e. biomethane, biohydrogen and biohythane). More in detail, while the anodic chamber was operated with the same operating conditions (i.e. electrodic material, HRT and OLR) throughout the experiment, different cathodic electrodic materials, inoculums and operation modes were changed to target the production of different reduced compounds. Indeed, the main novelty of the study consisted of examining different cathodic processes using the same bioanode, providing novel perspectives and possibilities in the field of bioelectrochemical processes development. During the overall experiment, the MEC was operated with a three-electrode configuration setting the anode potential at +0.20 V vs. SHE (Standard Hydrogen Electrode). The bioanode was fed continuously with synthetic wastewater and the chemical oxygen demand (COD) removal efficiency and the Coulombic Efficiency were studied to evaluate the anode performance. The first cathodic configurations consisted of granular graphite methanogenic biocathode for CH_4 production, in the second configuration a mixed metal oxide (MMO) electrode was utilized to evaluate abiotic H_2 production and in the third one the abiotic H_2 production was coupled with a CO_2 adsorption column to allow the production of bio-hythane, a mixture of biomethane with an H_2 content of 10% [32,33]. The different steady-state conditions were characterized by monitoring the different anodic and cathodic species concentrations over time. The utilization of mass, electron and energy balances then characterized each steady-state condition.

2. Materials and methods

2.1. Microbial electrolysis cell set-up

The MEC consisted of two-chamber filter-press configuration reactor. Both chambers (each 0.86 L) were made of Plexiglas and separated by a Nafion117 proton exchange membrane (Dupont, USA). Bioanode was set up using granular graphite electrode inoculated with activated sludge coming from a WWTP located in Treviso, Italy. Depending on the operating period, the cathodic electrodic material was constituted of graphite granules or by mixed metal oxide (MMO) electrode (Magneto special anodes, The Netherlands). Figure S1 shown the picture of the different type of electrodic materials and equipment adopted in the study. Moreover, according to the desired cathodic product, anaerobic digestate was adopted as inoculum in the cathodic chamber. The MEC was connected to a potentiostat (Ivium-nStat, multichannel electrochemical analyzer) controlling the anodic potential at + 0.20 V vs. SHE with a three electrodes configuration. According to the three-electrode configuration, the anode constituted the working electrode (WE), while the cathode constituted the counter electrode (CE). The reference electrode, present in each chamber of the MEC to ensure potentiostatic control (at the anode) and a measurement of the cathodic potential in the cathodic chamber. Both reference electrodes were an Ag/AgCl electrode, utilizing a KCl saturated solution (E = + 199 mV vs. SHE, Standard Hydrogen Electrode, Amelchem, Italy). The electrodic material of the anodic compartment consisted of granular graphite (Faima srl, Italy) which performed both the function of biofilm growth support and high surface electrode. The anodic chamber was continuously fed at 1.5 L/d, corresponding to a hydraulic retention time (HRT) of 0.57 d, through a peristaltic pump with a synthetic wastewater that simulate the composition of municipal wastewater. The synthetic wastewater composition was: Peptone (0.28 g/L), Yeast extract (0.15 g/L), glucose (0.68 g/L), sodium acetate (0.21 g/L), K_2HPO_4 (4.00 g/L), NH_4HCO_3 (0.19 g/L), $MgCl_2$*6 H_2O (0.10 g/L), $CaCl_2$*2 H_2O (0.05 g/L), Metals solution (10 mL/L) [34], Vitamins solution (1 mL/L) [35]. Moreover, two additional peristaltic pumps were used to recirculate anolyte and catholyte ensuring a complete mix of the two liquid phases. The different compartments were connected by Tygon® R3603 tubes to avoid the permeation of oxygen.

The five different MEC's operating period cathodic configuration are reported in Table 1.

During the first, third, fourth and fifth run, a gaseous mixture containing 70–30%(v/v) N_2/CO_2 was continuously fed in the cathodic chamber to simulate a biogas coming from an anaerobic digestor. In this way, the system was working with an inert gas with a Henry's constant comparable to the one of CH_4, such as nitrogen, and to work with a content of CO_2 comparable with a biogas CO_2 percentage. The outlet gas flow rate from the cathodic chamber was measured by a Milligascounter (Ritter, Germany). The feeding solution and the liquid and gaseous outlet of the anodic chamber was collected in a 10 L Tedlar® bag (Supelco, USA).

During the first operating period (Fig. 1-A), the cathodic chamber was addressed to stimulate the bioelectromethanogenesis reaction, i.e. the CH_4 production from CO_2 reduction by using a graphite granules biocathode. The cathodic chamber was filled with granular graphite (diameters from 6 to 2 mm) and of real density equal to 2.0 g/mL. The cathodic chamber was filled with mineral medium with the following composition: K_2HPO_4 (4.00 g/L), NH_4HCO_3 (0.19 g/L), $MgCl_2$*6 H_2O (0.10 g/L), $CaCl_2$*2 H_2O (0.05 g/L), Metals solution (10 mL/L). The cathodic inoculum consisted of a pretreated digestate coming from an anaerobic digestor located in Treviso (Italy). The digestate pretreatment consisted of the substitution of the supernatant solution obtained after solid sedimentation. The substitution of the liquid phase with mineral medium was repeated three times before proceed with the inoculum of the cathodic chambers.

The second configuration (Fig. 1-B), adopted from the second operating period was set-up to investigate the abiotic H_2 production by abiotic cathode.H_2 was collected in 5 L Tedlar ® bag. In this operating period, the graphite granules were replaced in the cathode by a square-shaped mesh electrode consisting of Mixed Metal Oxides (MMO) (Magneto special anodes, The Netherlands), connected to the circuit by a titanium wire. The cathodic chamber was filled with PP plastic cylinders to ensure similar mechanical properties of the cathodic chamber. During this experimental period no N_2/CO_2 gaseous mixture was fed to the cathodic chamber.

During the third and fourth operating period (Fig. 1-C), cathodic chamber was connected to a 2 L CO_2 sorption chamber. The CO_2 sorption chamber was hydraulically connected with the cathodic chamber by the continuous recirculation of the catholyte, moreover, CO_2 sorption chamber was continuously bubbled with the N_2/CO_2 gaseous mixture to promote CO_2 sorption in the alkaline catholyte. The objective of this configuration was the "theoretical" biohythane production, i.e. the production of a mixture of CH_4 and H_2 with a CO_2 content below 5%. Two different gaseous retention time (GRT) in the CO_2 sorption chamber

Table 1
Cathodic configuration and material during the experimental periods.

Operating period	1st	2nd	3rd	4th	5th
Target product	Biomethane	Hydrogen	Biohythane	Biohythane	Biomethane
Cathodic material	Graphite granules	MMO	MMO	MMO	MMO
Influent gas	N_2/CO_2 (70–30% *v/v*)	-	N_2/CO_2 (70–30% *v/v*)	N_2/CO_2 (70–30% *v/v*)	N_2/CO_2 (70–30% *v/v*)
CO_2 Adsorption chamber	-	-	2 L GRT 1 h	2 L GRT 6 h	-
Inoculum	Anaerobic digestate	-	-	-	Anaerobic digestate

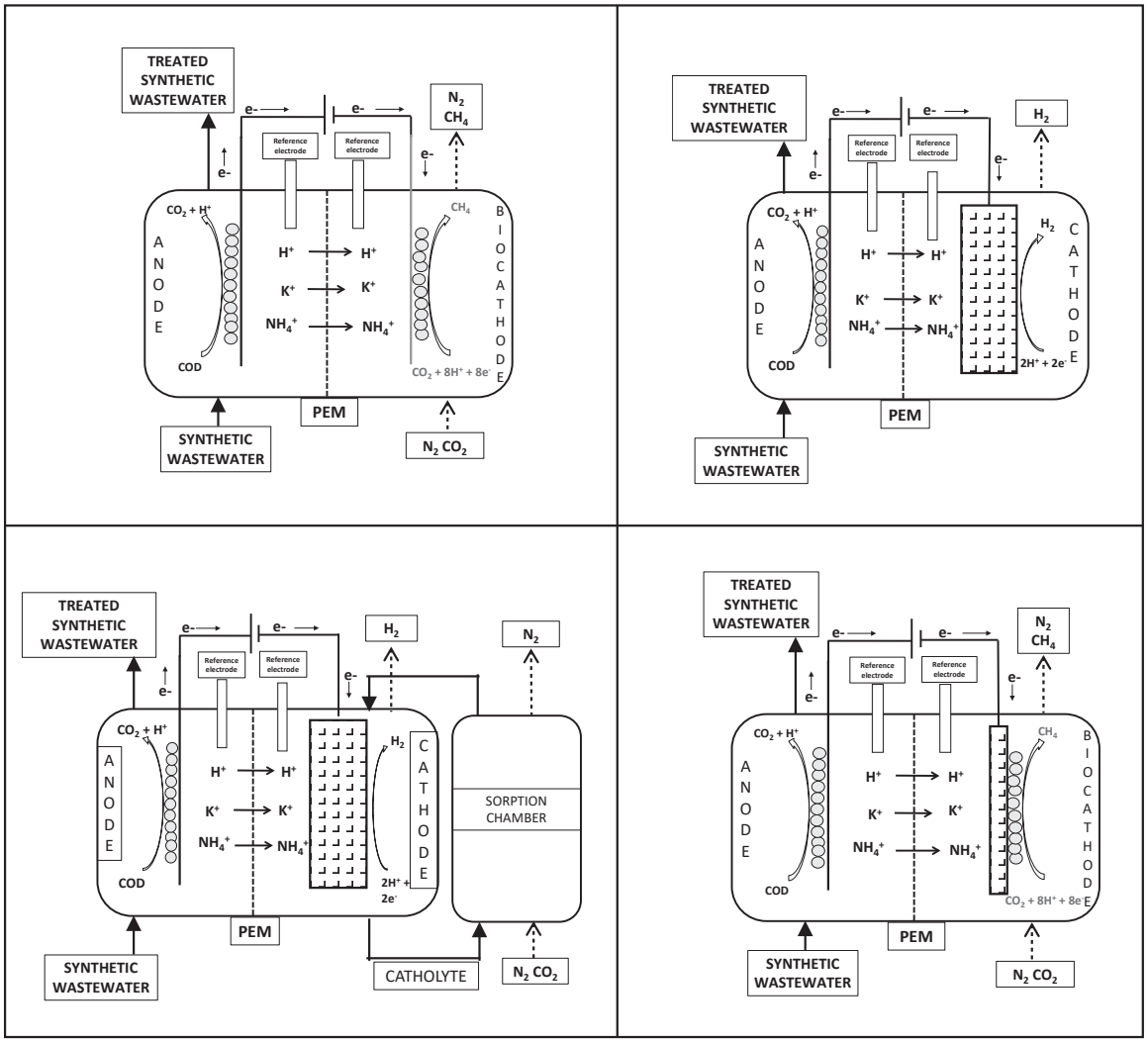

Fig. 1. Schematic representation of the bioelectrochemical configurations utilized in the experimental study: graphite granules biocathode (A), MMO electrode for abiotic hydrogen production (B), MMO electrode for abiotic hydrogen production+CO_2 sorption (C), MMO electrode for hydrogen mediated bio-electromethanogenesis (D).

was regulated by the influent N_2/CO_2 gaseous mixture flow rate.

During the fifth experimental period (Fig. 1-D), the cathodic chamber was inoculated with anaerobic digestate coming from the same full scale anaerobic digestor utilized in the first experimental period. Moreover, in this configuration the CO_2 sorption chamber was removed, and the N_2/CO_2 gaseous mixture was directly fed inside the cathodic chamber, in order to replicate the first condition with a different cathodic material.

2.2. Analytical methods

To determine the COD of the pre-filtered liquid phases, Spectroquant ® COD Cell Test, Supelco® and an UV–visible spectrophotometer (Shimadzu, λ 605 nm) were used. CH_4, H_2 and CO_2 determination was performed by injecting 50 µL of gaseous sample into a DaniMAster gaschromatograph (stainless-steel column packed with molecular sieve; N_2 as carrier gas 18 mL/min; oven temperature 70 °C; equipped with thermal-conductivity detector (TCD) temperature 150 °C). The inorganic carbon was measured by TOC (Total Organic Carbon Analyzer)-V CSN (Shimadzu) on filtered samples (ø 0.2 µm). The concentration of volatile suspended solids (VSS) was measured using GF/C filter (47 mm diameter, 1 µm porosity) following the APHA-AWWA-WPCF (1992) procedure. The Nessler method was used to determine spectrophotometrically (λ 420 nm) the concentration of ammonium ion. Potentials

are measured by a multimer (AM-520-EUR, Amprobe), pressure was measured by a digital pressure meter (DIgitron 2025 P, digital pressure meter), pH was monitored by a pH meter (Crison, GLP 22) equipped with a glass electrode (SlimTrode, CH-7402 Bonaduz, Hamilton). The average current was calculated recording the overall charge by the Ivium-nStat potentiostat.

2.3. Parameters and calculations

2.3.1. Anodic and cathodic parameters calculation

The removed COD was calculated the Eq. 1.

$$COD_{removed} = F * (COD_{in} - COD_{out}) \quad (1)$$

in which COD_{in} (mg/L) and COD_{out} (mg/L) represent respectively the anodic influent and effluent COD while F(L/d) is the influent and effluent flow rate in the anodic chamber (L/d).

The COD removal efficiency was calculated with the Eq. 2.

$$COD_{removal \quad efficiency} = \frac{(COD_{in} - COD_{out})}{COD_{in}} \quad (2)$$

The COD converted into electric current was expressed as electrons' equivalents, considering the water oxidation reaction (Eq. 3.)

$$2H_2O \rightarrow O_2 + 4e^- + 4H^+ \quad (3)$$

The meq_{COD} was calculated by using a theoretical conversion factor of 0.125 (4 meq/32 mgO_2).

The anodic Coulombic Efficiency (CE%) was calculated according to Eq. 4:

$$CE = \frac{meq_i}{meq_{COD}} \quad (4)$$

The cumulative electric charge (meqi) was calculated by integrating the current (A C/s) over time and dividing it by the Faraday's constant (F = 96,485 C/eq).

The production rate of methane $rCH_{4(mmol)}$ and hydrogen $rH_{2(mmol)}$ were determined considering the measured concentration of H_2/CH_4 inside the gaseous outlet (mmol/L), the gaseous flow (L/d), the time passed between the measures and the total operational time according to Eqs. 5a and 5b.

$$r_{CH_4} = \frac{\sum_0^n ([CH_4]_n * Qcat_{(out)n} * \Delta t_n)}{\Delta t_{tot}} \quad (5a)$$

$$r_{H_2} = \frac{\sum_0^n ([H_2]_n * Qcat_{(out)n} * \Delta t_n)}{\Delta t_{tot}} \quad (5b)$$

The methane and hydrogen production rates rH_2, rCH_4 (mmol/d) was also expressed in terms of equivalents (i.e. Eqs. 6a and 6b) $rCH_{4(meq)}$ $rH_{2(meq)}$ (meq/d), considering the theoretical conversion factor of 8 meq/$mmol_{CH4}$, and 2 meq/$mmol_{H2}$

$$rCH_{4(mmol)} * 8 = rCH_{4(meq)} \quad (6a)$$

$$rH_{2(mmol)} * 2 = rH_{2(meq)} \quad (6b)$$

The Cathode Capture Efficiency (CCE, %) was calculated by the ratio between the cumulative equivalents of produced methane (meq_{CH4}) in a fraction of time and the cumulative as expressed by Eqs. 7a and 7b:

$$CCE = \frac{meq_{CH4}}{meq_i} \quad (7a)$$

$$CCE = \frac{meq_{H2}}{meq_i} \quad (7b)$$

2.3.2. Inorganic and ammonium mass balance calculation

The daily removal of CO_2 (ΔCO_2, mmol/d) inside the cathodic chamber has been evaluated by the Eq. 8.

$$\Delta CO_2 = Qcat_{in} * CO_{2in} - Qcat_{out} * CO_{2out} \quad (8)$$

In which Q_{cat}in (L/d) and Q_{cat}out (L/d) are the influent and effluent gas flow rates, respectively., while, CO_2in and CO_2out (mmol/L) represent the CO_2 concentrations in the influent and effluent gaseous cathodic streams, respectively.

The Eq. 9 represents the CO_2 removal efficiency calculation:

$$CO_2 removal \quad efficiency(\%) = \frac{Qcat_{in} * CO_{2in} - Qcat_{out} * CO_{2out}}{Qcat_{in} * CO_{2in}} \quad x100 \quad (9)$$

The daily nitrogen removal (ΔN; mg/d) has been evaluated by the Eq. 10.

$$\Delta N = F_{in} * N_{\quad in} - F_{out} * N_{\quad out} \quad (10)$$

In which F_{in} and F_{out} (L/d) are the influent and effluent liquid flow rates, respectively. Moreover, N_{in} and N_{out} (mg/L) represent the nitrogen concentration inside the inlet and outlet of the anodic chamber. Since the nitrogen was in form of ammonium, it could migrate through the CEM, and it was detected inside the cathodic chamber where it was recovered inside the catholyte daily spill, i.e. the daily amount of liquid phase migrating from the anode to the cathode due to the electroosmotic phenomenon. A small portion of ammonium is used by microorganisms for growth, indeed, according with the generic biomass composition ($C_5H_7O_2N$) a 0.12 factor was taken into consideration for the overall nitrogen mass balance, expressed by Eq. 11:

$$(F_{in} * N_{in} = F_{spill} * \left(VSS_{out \quad cat} * 0.12 \frac{g_N}{g_{VSS}} + N_{\mathrm{Cat}} \right) + F_{out} * (N_{\mathrm{out}} + VSS_{\mathrm{out\ anode}} * 0.12 \frac{g_N}{g_{VSS}}) \quad (11)$$

In which F_{in} and F_{out} (L/d) are the influent and effluent liquid flow rates, respectively. Moreover, N_{in} and N_{out} (mg/L) represent the nitrogen concentration inside the inlet and outlet of the anodic chamber. N_{cat} represent the nitrogen concentration (mg/L) inside the cathodic chamber and F_{spill} is the daily spill (L/d) from the cathodic chamber; VSS_{out} is the measured concentration (mg/L) of the volatile suspended solid ($C_5H_7O_2N$) inside the anodic or cathodic effluent, 0.12 is the conversion factor used for determining the ammonium nitrogen used for the biomass growth (mgN/mgVSS).

2.3.3. Energy balance calculations

The energy efficiency (ηE) was calculated considering the energy theoretically recoverable from the combustion of the produced methane (W_{CH4}) or/and hydrogen (W_{H2}) and the energetic consumption of the system (W_{in}) as expressed by Eq. 12:

$$\eta E = \frac{W_{CH4} + W_{H2}}{W_{in}} = \frac{r_{CH4(mmol)} \times \Delta G_{CH4} + r_{H2(mmol)} \times \Delta G_{H2}}{\Delta V \times i} \quad (12)$$

where ΔGCH_4 (−817.97 KJ/mol), ΔGH_2 (−286 KJ/mol) and $rCH_{4(mmol)}$ (mmol/d) and $rH_{2(mmol)}$ represent the molar Gibbs free energy for methane/hydrogen combustion and the methane/hydrogen production rate, respectively; ΔV is the difference of potential established between the counter and the working electrodes (i.e., cell voltage), and i represents the average current flowing in the reactor.

The energetic consumptions for CO2 and COD removal were determined by Eq. 13 as follows.

$$EC(kWh / Nm^3CO_2) = \frac{kWh}{\Delta CO_{2(Nm3/d)}} = \frac{\Delta V * i * 24(h/d)}{\Delta CO_{2(Nm3/d)}} \quad (13)$$

Where ΔCO_2 is the daily removal of CO_2 (Nm^3/d), ΔV is the potential difference measured between anode and cathode (V), i is the electric

current registered (A). To estimate the energetic consumption for CO_2 removal considering the energy spared (1.2 kWh/kgCOD [36]) for the COD removal, taking into account that this system carries out two processes with only one energetic consumption, Eq. 14 was changed as follows in Eq. 14.

$$EC_{COD}(kWh/Nm^3CO_2) = EC_{CO_2} - 1.2\eta_{COD} \quad (14)$$

In which η_{COD} represents the amount of COD removed per mole of CO_2 removed.

2.3.4. Potential losses characterization

The following Eq. 15 was used to calculate the potential loss $\sum \eta$ (V) which represent the sum of the overpotentials.

$$\sum \eta = \Delta V_{(exp)} - \Delta V_{(meas)} \quad (15)$$

ΔV_{exp} is the difference of potential measured between the cathode and the anode during the experiment and ΔV_{meas} represent the calculated potential difference according to the Eq. 16

$$\Delta V_{(meas)} = E_{cath(meas)} - E_{an(meas)} \quad (16)$$

In which $E_{cath(meas)}$ and $E_{an(meas)}$ are the measured potential vs the reference electrode placed in the respective chamber. The following Eq. 17 was used to calculate the cathodic potential loss $\sum \eta_{cat}$ (V) which represent the sum of the cathodic overpotential.

$$\sum \eta_{cat} = E_{cath}^{meas} - E_{cath}^{th} \quad (17)$$

In which E_{cath}^{meas} is the measured value during the experimental period whereas E_{cath}^{th} represent the theoretic value calculated with the Nernst Eq. (18)

$$E_{cath}^{th} = E^0 - \frac{RT}{2F}\ln\frac{pH_2}{[H^+]^2} \quad (18)$$

In which E° for H^+/H_2 is equal to 0 V, F is the Faraday's constant (96,485 C/mol_e-), R is the universal gas constant (8.314 J/molK), and T is the temperature expressed in Kelvin. The pH_2 used is $10^{-3.1}$ atm which corresponds to 8 mM which is the maximum solubility of hydrogen in water with atmospheric pressure and normal temperature (25°C). The pH_2 used for the first and last period is 10^{-4} atm which is the maximum hydrogen's partial pressure on which methanogens work. The same statement can be made for the anodic reaction and the anodic overpotential (Eq. 19).

$$\eta_{an} = E_{an(meas)} - E_{an(eq)} \quad (19)$$

Equilibrium potential of the anodic potential is determined by Eq. 20.

$$E_{anCOD\ (eq)} = E^0 + \frac{RT}{8F}\ln\frac{[HCO_3^-]^2 * [H^+]^9}{[CH_3COO^-]} \quad (20)$$

In which E° for HCO_3^-/CH_3COO^- is equal to + 0.187 V vs SHE, F is the Faraday's constant (96,485 C/mol_e-), R is the universal gas constant (8.314 J/molK), and T is the temperature expressed in Kelvin.

The potential losses linked to the pH gradient (Eq. 21) and to the electrolyte resistance (Eq. 22) were calculated as reported in the literature [37].

$$\eta_{pH} = \frac{RT}{F}\ln(10^{(pH_{cathode} - pH_{anode})}) \quad (21)$$

In which, as in the Eq. 17, F is the Faraday's constant (96,485 C/mol_e-), R is the universal gas constant (8.314 J/molK), and T is the temperature expressed in Kelvin.

$$\eta_{ionic} = I_{ions}\left(\frac{1}{2}R_{anode} + \frac{1}{2}R_{cathode}\right) = I_{ions}\left(\frac{d_{an}}{2A\sigma_{an}} + \frac{d_{cat}}{2A\sigma_{cat}}\right) \quad (22)$$

I_{ions} represent the amount of charges migrated through the membrane (the value is the same of the registered electric current $\frac{C}{s}$ = A), R is the resistance of the liquid phase which can be calculated knowing the distance "d" of the electrode from the membrane (cm), the membrane's area "A" (cm^2) and the conductivity ($\frac{S}{cm}$) of the liquid phase. While σ_{an} and σ_{cat} have been experimentally determined by a conductometer, the distance between the proton exchange membrane and the electrode has been assumed equal to 1.5 cm (which represent the middle of the chamber), in each explored configuration.

3. Results and discussion

3.1. Anodic performance of the anodic chamber during the different operating periods

After the start up period the anodic biofilm was operated for 5 months applying the same operating conditions, i.e., a theoretical organic load rate of 2 gCOD/Ld and a hydraulic retention time of 0.57 days, showing stable electroactive activity despite the cathodic operating conditions shifts (i.e., electrodic material, electrolyte pH), highlighting the resilience of the anodic biofilm. The influent and effluent COD concentration time course in the anodic chamber is shown in Figure S2. During the first period operating period (graphite granules biocathode addressed to biomethane production), the average electric current generated by the oxidation of COD was 51 ± 5 mA (Fig. 2) while the COD removal was 981 ± 35 mgCOD/d. The resulting CE was 37 ± 3% and indicated a low conversion efficiency of the electrons produced by the COD oxidation into current. After 37 days the granular graphite biocathode was substitute with a mixed metal oxide (MMO) electrode inserted in polypropylene packed bed. Even though MMO electrodes are usually adopted for water oxidation in several of bioelectrochemical applications [38], the presence of several noble metals was investigated for the hydrogen evolution reaction [39]. Those operation did not shock the anodic biofilm, indeed, during the second operating period the bioanode coulombic efficiency increased to 45 ± 4%, due to an average daily COD removal of 929 ± 35 mgCOD/d and an average current of 58 ± 5 mA. As expected, during the fourth and fifth operating condition, the insertion of the CO_2 sorption chamber did not affect the anodic biofilm activity, indeed, as reported in Table 2, the daily COD removal and current value remained similar, confirming again the possibility to tune MEC's anodic and cathodic performances separately. However, during the last investigated period, after the reinoculation of the cathodic chamber with the pretreated anaerobic digestate, the anodic biofilm increased the current production to an average value of 111 ± 15 mA removing the same amount of COD (972 ± 33 mgCOD/d) showing a higher CE of 82 ± 5%.

3.2. Biofuels production during the different cathodic operating periods

The first experimental period, in which a granular graphite biocathode was adopted for CO_2 reduction into CH_4, showed a methane production rate of 26 ± 4 meq/d of CH_4 which corresponded to a cathodic coulombic efficiency (CCE) of 59 ± 4%. The experimental results were in line with previous data reported for similar methanogenic biocathode [21], which also reported an incomplete current recovery into methane, suggesting the presence of unknown reductive reactions. In order to change the cathodic product from biomethane to hydrogen, the cathodic granular graphite colonized by the methanogenic biofilm was substitute with a commercial mixed metal oxide (MMO) electrode that was inserted in a polypropylene packing material physically supporting the ion exchange membrane. Even if MMO electrodes are usually utilized for oxygen evolution by water electrolysis [40], the presence of noble metal catalysts on its surface suggests its applicability as cathodic material. During this second operating period, no inoculum was inserted in the cathodic chamber to promote the abiotic hydrogen production. As reported in Fig. 3, an average hydrogen production rate of 14 ± 2 meq/d

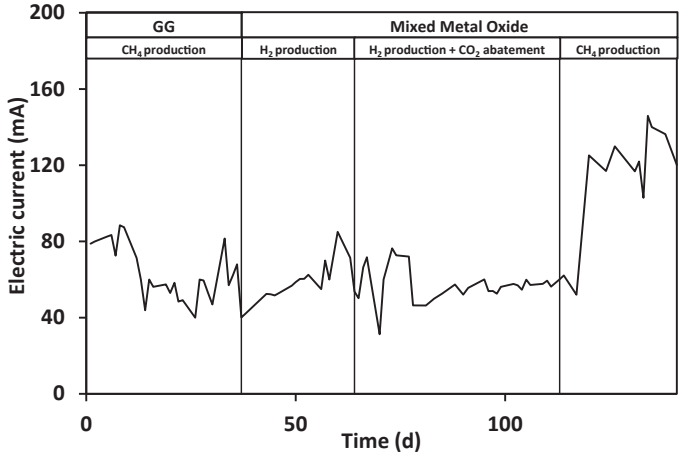

Fig. 2. Electric current generated by the anodic biofilm during the experimental periods.

Table 2
Summary of the anodic performance during the 4 experimental periods.

Cathode Goal	GG CO_2 reduction into CH_4	MMO H_2 production	MMO H_2 production + CO_2 abatement GRT 1 h	MMO H_2 production + CO_2 abatement GRT 6 h	MMO CO_2 reduction into CH_4
Electric current (mA)	51 ± 5	58 ± 5	56 ± 4	56 ± 4	111 ± 15
COD removal (mgCOD/d)	981 ± 35	929 ± 35	695 ± 35	695 ± 35	972 ± 33
CE	37 ± 3%	44 ± 3%	57 ± 3%	57 ± 3%	82 ± 5%

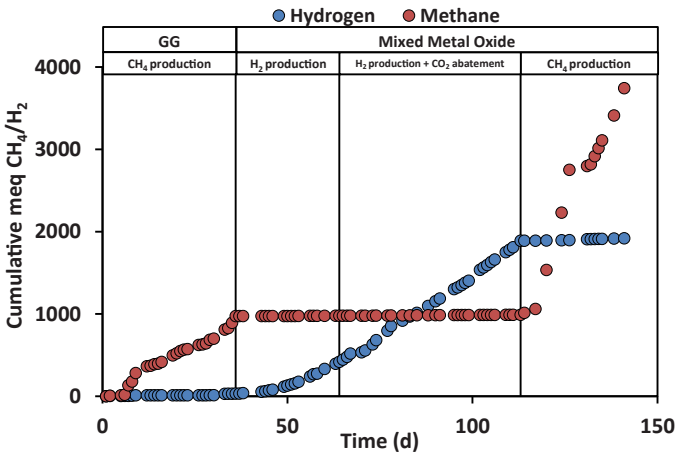

Fig. 3. Cumulative milliequivalents of the cathodic products.

was recorded giving an average CCE of 27 ± 3%. This low performance was mainly caused by an unexpected low H_2 concentration in the Tedlar gas bag utilized for hydrogen quantification during this period, indeed, only a volumetric hydrogen concentration of 57 ± 5%was recorded by GC analysis. According to analytical characterization a N_2/O_2 ratio was also present in the gas composition probably due to air retro diffusion in the gas bag collector. The progressive proton consumption from the cathodic chamber and the simultaneous migration of species different from protons generates alkalinity inside the catholyte which promoted the increase of the catholyte pH till the value of 13.5 ± 0.8. The cathodic potential did not change significantly showing an average value of - 0.9 ± 0.1 V vs SHE, moreover, the cathodic conductivity, was significantly lower than the one measured during the first experimental period (i.e., 11 ± 2 mS/cm vs 116 ± 10 mS/cm) according to the lack of bicarbonate generation due the CO_2 sorption. In order to integrate the CO_2 sorption process for biogas upgrading, during the 3rd operating period a 1.2 L sorption chamber, consisting of a borosilicate glass flask, has been integrated with the cathodic chamber process (Fig. 1-D) Sorption chamber was operated having the catholyte continuously recirculated while the N_2/CO_2 gas mixture was bubbled in the sorption glass chamber. The integration of the cathodic chamber with the sorption chamber allowed to obtain two separate gaseous streams: one coming out the cathodic chamber, the second coming out the sorption chamber. During the first operating period with the sorption chamber configuration, i.e., the third operational period, a N2/CO2 flow rate of 32 ± 1 L/d was fed in the sorption chamber, corresponding to a GRT of 1 h of the gaseous phase. During the 1 h GRT, as expected, the CO_2 sorption promoted the catholyte pH decrease to an average value of 8.6 ± 0.5, while the catholyte conductivity raised to 60 ± 4 mS/cm. During the 1 h GRT, the H_2 production stabilized at an average value of to 29 ± 3 meq/d resulting in a CCE of 58 ± 5% (volumetric H_2 concentration of: 66 ± 5%). To reduce the CO_2 load rate in the sorption chamber, and obtain a lower CO_2 concentration, during the 4th operating period, the gaseous N_2/CO_2 flow rate was decreased to 5 ± 1 L/d, resulting in a GRT in the sorption chamber of 6 h. The catholyte's pH increased to 9.4 but the cathodic potential and the catholyte's conductivity did not change significantly. The results of the GRT increase were a higher H_2 volumetric concentration of 86 ± 6% and a lower CO_2 concentration of 4 ± 1%. After those promising results, the glass bottle was removed (the gaseous mixture was bubbled directly inside the cathodic chamber), and the cathodic chamber, containing the MMO electrode and the polypropylene packing material was inoculated with a methanogenic inoculum. During the last operating period, the inoculated cathodic camber produced methane with a production rate of 102 ± 8 meq/d giving a CCE of 102 ± 4%. This result is significantly higher than the one obtained with graphite granules as cathodic material. Probably, even if the graphite granules have a higher superficial area and the MMO is a particular electrodic material (more expensive than graphite granules) the MMO is more suitable for hydrogen production and therefore more suitable for hydrogenophilic

Table 3
Summary of the cathodic performance during the 4 experimental periods.

Cathode Goal	GG CO_2 reduction into CH_4	MMO H_2 production	MMO H_2 production + CO_2 abatement GRT 1 h	MMO H_2 production + CO_2 abatement GRT 6 h	MMO CO_2 reduction into CH_4
Electric current (mA)	51 ± 5	58 ± 5	56 ± 4	56 ± 4	111 ± 15
r_{H_2} (meq/d)	1 ± 1	14 ± 2	29 ± 3	31 ± 3	1 ± 1
r_{CH_4} (meq/d)	26 ± 4	-	-	-	102 ± 8
CCE %	59 ± 4	27 ± 3	58 ± 5	62 ± 5	102 ± 4

methanogens. Table 3

3.3. Inorganic carbon mass balance

During each operating period the inorganic carbon was monitored in the anodic and cathodic liquid and gaseous phases. During the first operating period, in which graphite granules were adopted as cathodic electrodic material, the inorganic carbon concentration in the catholyte quickly stabilized at 16 ± 1 gCO_3^{2-}/L, a considerably higher concentration with respect to the inorganic carbon concentration in the anodic chamber which resulted on average 1 ± 1 gCO_3^{2-}/L. Inorganic carbon concentration increase was correlated with the CO_2 sorption in the catholyte, which corresponded to an average CO_2 removal of 89 ± 4 mmol/d. The corresponding CO_2 removal efficiency resulted of 59 ± 2% obtained with a gaseous retention time (GRT) of 2 h. The CO_2 sorption phenomenon was driven by the alkalinity generation inside the cathodic chamber which was buffered by the CO_2 sorption as HCO_3^-/CO_3^{-2}. Moreover, as shown in Fig. 4, the anodic chamber acidification promoted a bicarbonate's concentration decrease, indeed, part of the influent bicarbonate in the anodic chamber was transformed in carbonic acid, with a consequent release of carbon dioxide. As reported in Table 4, similar trends of bicarbonate concentration and CO_2 removal were confirmed during each operating period. Interestingly, after the cathodic material change from graphite granules to MMO an operating period which did not involve the supply of the N_2/CO_2 gaseous mixture inside the cathodic chamber; the bicarbonate concentration in the catholyte did not increase resulting on average: 1.7 ± 0.2 g CO_3^{-2}/L. The third operating period, which involved the catholyte integration with the CO_2 sorption chamber continuously bubbled with the N_2/CO_2 gas mixture was divided in two different operating periods characterized by different gas retention times (GRTs), obtained respectively by using two different N_2/CO_2 flow rates, i.e. GRT of 1 h was obtained by a flow rate of 32 ± 1 L/d; while a 6 hour GRT was obtained using a flow rate of 5 ± 1 L/d. During the 1 h GRT operating period, the CO_2 removal was on average 143 ± 21 mmol/d corresponding to a CO_2 removal efficiency of 40 ± 4%. On the other hand, increasing GRT to 6 h decreased the CO_2 removal CO_2 removal rate 49 ± 5 mmol/d while increasing the CO_2 removal efficiency to 85 ± 6%. During the GRT 1 h operation the CO_2 concentration in the sorption chamber outlet was 20 ± 4% while, the GRT increase to 6 h allowed to obtain a CO_2 concentration in the outlet gaseous phase of 5 ± 2%. The catholyte bicarbonate concentration was not affected by the change of gas mixture GRT, remaining stable to an average value of 33 ± 2 gCO_3^{2-}/L. During the last MEC's operating period, in which anaerobic sludge has been inoculated in the cathodic chamber equipped with the MMO electrode, the sorption chamber was removed and a direct GRT of 1 h (corresponding to a flow rate 21 ± 2 L/d) was applied to the cathodic chamber. During this period the catholyte bicarbonate concentration reached 8.5 ± 0.8 g/L, giving an average the CO_2 removal of 70 ± 3 mmol/d and a CO_2 removal efficiency of 26 ± 3%.

Table 4
Summary of the inorganic carbon mass balance during the 4 experimental periods.

Cathode Goal GRT (h)	GG $CO_2 \rightarrow CH_4$ 2	MMO $H^+ \rightarrow H_2$ 1	MMO $H^+ \rightarrow H_2$ 6	MMO $CO_2 \rightarrow CH_4$ 1
Electric current (mA)	51 ± 5	58 ± 5	56 ± 4	111 ± 15
CO_2 removal (mmol/d)	89 ± 4	143 ± 21	49 ± 5	70 ± 3
CO_2 removal efficiency %	59 ± 2%	40 ± 4%	85 ± 6%	26 ± 3%

3.4. Nitrogen mass balance

During each operating, ammonium concentration in all reactor's liquid phases (anodic influent, anodic effluent, cathodic chamber) was

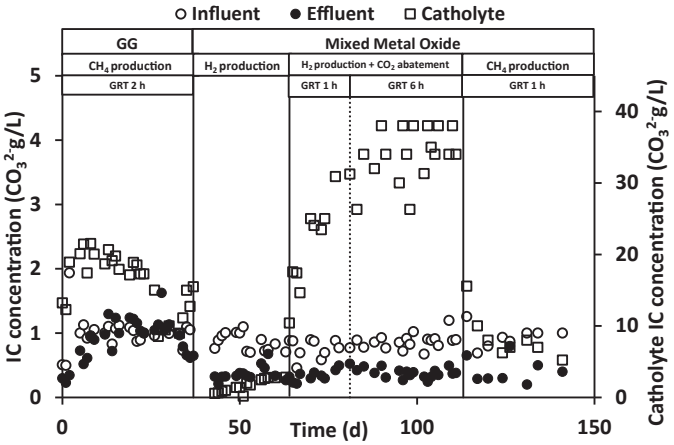

Fig. 4. Inorganic carbon concentrations inside the liquid phases during the four experimental periods.

monitored. Cations were able to migrate through the cation exchange membrane in every experimental period. Electroneutrality was maintained by this migration from the anodic chamber to the cathodic one. This migration can be harnessed to remove nitrogen from wastewater, which is essential for efficient wastewater treatment and preventing eutrophication. Nitrogen levels were monitored during each experimental period to assess performance. It's worth noting that the volume of volatile suspended solids (VSS) exiting the anodic chamber, in the case of a biological cathode, did not change significantly. Therefore, the amount of nitrogen removed through microbial growth can be considered consistent across all experimental periods. This suggests that the cathodic biomass was not affected by changes in the cathodic material. Furthermore, as shown in Table 5, nitrogen removal through microbial growth inside the cathodic chamber did not make a significant contribution. On the other hand, the experimental periods with a Mixed Metal Oxide (MMO) cathode exhibited higher nitrogen removal rates (58 ± 4%) compared to graphite granules (40 ± 3%). This performance is attributed to the higher nitrogen concentration inside the catholyte during the last three experimental periods compared to the first one, which used graphite granules as the cathodic material. As shown in Fig. 5, the increased electric current obtained during the last experimental period did not significantly change the ammonium concentration in the catholyte. Therefore, the presence of the proton exchange membrane and its specific fixed charge plays a fundamental role in this process along with the presence of more homogenous electrodic materials, indeed, the electric field generated by MMO cathodes with respect graphite granules could explain the higher nitrogen removal rate obtained. Therefore, in addition to the presence of more homogenous electrodic materials (i.e. MMO electrode with respect GG), the presence of the proton exchange membrane and its specific fixed charge plays a fundamental role in this process which could influence the nitrogen removal rate. Anyway, the major takeaway is that significant nitrogen removal from wastewater can be achieved using a proton/cation exchange membrane dividing anodic and cathodic chamber. These results are obtained without any additional energy consumption, which is a significant advantage when considering that ammonium nitrogen is typically removed through air stripping, requiring 9 kWh/kgN of energy [41].

3.5. Potential losses characterization

Throughout the duration of the experiment, the anodic potential was controlled at +0.2 V vs. SHE, ensuring the control of the anodic overpotentials. On the other hand, the cathodic potential was allowed to change in response to the overall reaction rate, i.e. the current. The potential difference (i.e. the cell voltage) between the anode and cathode remained relatively stable during the first four operating periods.

Table 5
Summary of the nitrogen mass balance during the 4 experimental periods.

Cathode Goal	GG $CO_2 \rightarrow CH_4$	MMO $H^+ \rightarrow H_2$	MMO $H^+ \rightarrow H_2 + CO_2$ abatement	MMO H_2 production + CO_2 abatement	MMO $CO_2 \rightarrow CH_4$
GRT (h)	2	-	1	6	1
N_{in} (mgN/d)	131 ± 5	223 ± 15	260 ± 13	264 ± 14	103 ± 5
N_{out} (mgN/d)	78 ± 5	96 ± 5	100 ± 3	104 ± 6	45 ± 3
N_{spill} (mgN/d)	16 ± 1	5 ± 1	3 ± 1	3 ± 1	32 ± 5
Anodic VSS_{out} (mgN/d)	16 ± 3	10 ± 4	8 ± 3	9 ± 3	9 ± 5
Cathodic VSS_{spill} (mgN/d)	1 ± 1	-	-	-	1 ± 1

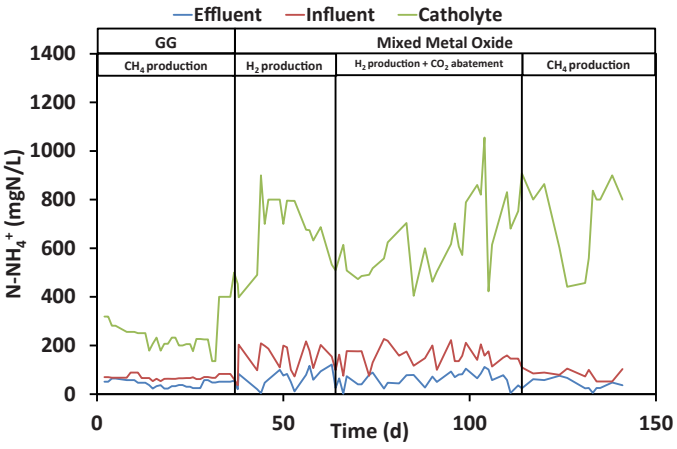

Fig. 5. Ammonium nitrogen concentrations inside the liquid phases during the four experimental periods.

However, in the last experimental period, there was a notable increase in the potential difference due to a significant rise in electric current (from 56 ± 4–111 ± 15 mA) (Figure S3). The equilibrium cathodic potential ($Ecat_{eq}$) was calculated during both the first and last experimental periods using Eq. 18 and adjusted according to variations in pH. As a result, during the second experimental period, the cathodic equilibrium potential was significantly higher than that calculated for the other four periods (−0.7 vs. −0.4 V vs. SHE). Interestingly, the measured cathodic potential did not change as anticipated by the calculations, measuring at −0.87 ± 0.10 V vs. SHE at pH 13.49 ± 0.14 and −0.81 ± 0.11 V vs. SHE at pH 8.57 ± 0.14. It's worth noting that the cathodic potential did change when the cathodic material was altered, transitioning from graphite granules to mixed metal oxide. The first and fifth operating periods used the same experimental conditions, but the cathodic potential measured during the first period was slightly lower than that measured during the last period (−0.90 ± 0.11 vs. −0.78 ± 0.15 V vs. SHE). This result is likely due to the different materials used, as each experimental period led to lower cathodic overpotentials than those observed with graphite granules (Figure S4). Additionally, the ionic overpotential changed significantly only during the last experimental period due to lower catholyte conductivity, caused by a decrease in ionic concentration, as shown in Fig. 6. This drop in ionic concentration resulted from the activity of methanogens, which reduced the bicarbonate in the catholyte to methane, utilizing the reducing power generated at the cathode. Furthermore, the pH split overpotential tracked the pH variations within the cathodic chamber, as the anodic

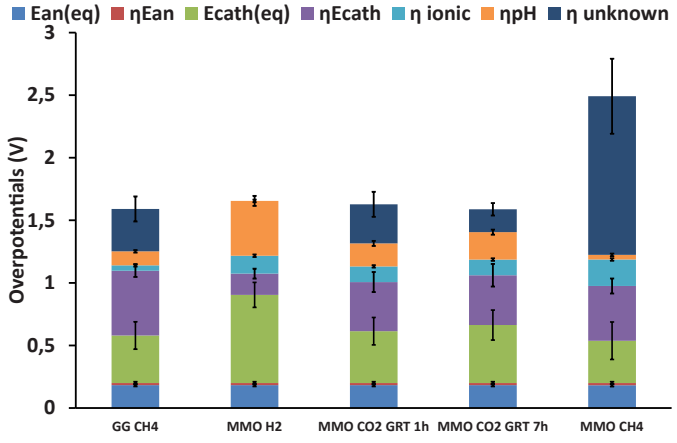

Fig. 6. Potentials and potential losses calculated and measured during the experimental periods.

chamber maintained a steady pH conducive to the growth of electroactive biofilm. In contrast, during the first and last conditions, the cathodic pH was regulated by introducing CO_2 to maintain an optimal pH for methanogen growth in the cathodic chamber. During the second experimental period, pH was not controlled, and the catholyte reached a pH of 13.49 ± 0.14, resulting in a pH split overpotential of 0.44 ± 0.04 V. During the third and fourth periods, CO_2 was bubbled into the glass chamber, lowering the pH. However, during the fourth period, with a lower flow rate (which means a longer GRT), the resulting pH was higher, leading to a higher pH split overpotential. Table 6 summarizes the overpotentials, demonstrating that a complex system like the MEC yields different results under various conditions.

3.6. Energy balance

The energy consumption was evaluated during each experimental period to determine the best condition from an energy and economic standpoint. As shown in Table 7, the potential differences were similar during the first four experimental periods. However, in the last period, it increased along with the electric current, which was double that of the previous four experimental periods. This led to an energy consumption almost four times higher than the one calculated for the first four periods (2 ± 1 vs. 7 ± 1 Wh/d). For this reason, in order to achieve comparable performance between the first four periods and the last one, it is necessary to either remove four times the CO_2 removed during the first four periods or produce four times the methane produced during the first period. Since the CO_2 removal in the last period was not as high as expected given the electric current, the energy consumption for that process is significantly higher than what was obtained with a lower electric current. Therefore, as shown in Table 7, the best experimental conditions for CO_2 reduction were those with a high flow rate (low GRT) and no inoculum inside the cathodic chamber. During this experimental period (the third one), the CO_2 reduction was the highest achieved (143 ± 21 mmol/d) with an energy consumption similar to the other three periods, at 2 Wh/d (resulting in 0.62 ± 0.05 kWh/Nm^3CO_2). If we consider the COD (Chemical Oxygen Demand) removed by the bioanode and knowing that 1 g COD is typically removed in a wastewater treatment plant with an energy consumption of 1.1 Wh, the net energy cost of CO_2 reduction is lower. This is possible because MECs energy consumption allows to run multiple processes in the anodic and cathodic chamber. Indeed, COD oxidation, CO_2 removal, and H_2/CH_4 production are carried out using the same energy provided by the applied potential. For this reason, even in the best case, the energy consumption per normal cubic meter of CO_2 removed is comparable (or even better) than the best available techniques (0.75 kWh/Nm^3CO_2 according to [36]). Taking into account COD reduction, this system proves to be more cost-effective for CO_2 removal. In conclusion, it is possible to recover the energy spent to sustain the system by exploiting the CH_4/H_2 produced. During the fourth experimental period, it was possible to recover 57 ± 3% of the energy spent by burning the H_2 produced. In the worst-case scenario, around 25 ± 3% (during the second period) could be recovered from H_2, and approximately 40% (39 ± 3% and 44 ± 5%) from CH_4.

Table 6
Potentials and potential losses calculated and measured during the experimental periods.

Cathode Goal	GG $CO_2 \rightarrow CH_4$	MMO $H^+ \rightarrow H_2$	MMO $H^+ \rightarrow H_2$ + CO_2 abatement	MMO H_2 production + CO_2 abatement	MMO $CO_2 \rightarrow CH_4$
GRT (h)	2	-	1	6	1
i (mA)	51 ± 5	58 ± 5	56 ± 4	56 ± 4	111 ± 15
ΔV (V)	- 1.59 ± 0.25	- 1.63 ± 0.28	- 1.63 ± 0.26	- 1.59 ± 0.25	- 2.49 ± 0.39
E_{cath} (V vs SHE)	- 0.90 ± 0.11	- 0.87 ± 0.10	- 0.81 ± 0.11	- 0.86 ± 0.12	- 0.78 ± 0.15
ηcath (V)	0.52 ± 0.05	0.17 ± 0.04	0.40 ± 0.08	0.40 ± 0.09	0.44 ± 0.06
ηpH (V)	0.11 ± 0.01	0.44 ± 0.04	0.18 ± 0.02	0.22 ± 0.02	0.04 ± 0.01
ηionic (V)	0.09 ± 0.01	0.14 ± 0.01	0.13 ± 0.01	0.12 ± 0.01	0.21 ± 0.01

4. Conclusions

The experimental study demonstrates the feasibility of using a bioanode to drive cathodic biofuel production through the combination of biological and physicochemical processes. During the long-term MEC operation, the anodic chamber of the MEC removed on average 855 ± 57 mgCOD/d producing an average electric current of 66 ± 7 mA and giving an average coulombic efficiency of 55 ± 5%. The cathodic performance was assessed for various operating conditions and process configurations to achieve different targets and applications. This included H_2 production, CO_2 removal from a gaseous stream, and biomethane production. The use of Mixed Metal Oxide (MMO) as electrodic material enabled the reduction of cathodic reaction overpotentials (i.e hydrogen evolution) as also described by the increase in biomethane production when anaerobic digestate was used as inoculum. Indeed, CH_4 production resulted in 26 ± 4 and 102 ± 8 meq/d with graphite granules and MMO electrode, respectively. Despite these remarkable results, the highest CO_2 removal (143 ± 21 mmol/d) was achieved with the "MMO abiotic cathode–sorption chamber" configuration using a GRT 1 h. However, the latter "MMO abiotic cathode-sorption chamber" configuration, needed a N_2/CO_2 GRT of 6 hours in order to get a CO_2 concentration lower than 5% v/v. This GRT increase to 6 h, reduced the daily CO_2 removal to 49 mmol/d but allowed for the achievement of a gaseous mixture consisting of 9% H2, 5% CO_2, and 80% N_2. Assuming N_2 is CH_4 coming from real biogas, a commercial biohythane was obtained using part of the energy contained in the wastewater by the overall bioelectrochemical process. A daily energy consumption of 7 Wh/d was used during the operation at 6 h of GRT allowing for the operation of three different processes (COD removal, CO_2 sorption, and H_2/CH_4 production), resulting in a specific energy consumption of 1.84 ± 0.13 kWh/Nm^3CO_2 for the CO_2 removal operation and 1.14 ± 0.12 kWh/kgCOD for the COD removal. In conclusion, this work demonstrates the resilience and versatility of Microbial Electrolysis Cells (MECs), in which anodic COD oxidation can support several cathodic processes by exploiting the residual chemical energy contained in waste organic compounds. The most promising investigated configuration resulted in H_2 production with the MMO electrode combined with CO_2 sorption. In this case, the gaseous composition and energy consumption were in accordance with the commercial standards for biohythane [42] and the available biogas upgrading technologies already available for upgrading biogas [43].

Funding information

The authors gratefully acknowledge the Italian National Institute for Insurance against Accidents at Work (Istituto Nazionale per l'Assicurazione contro gli Infortuni sul Lavoro, INAIL) for financial support of this research, in the frame of national Call BRiC 2022, Piano Attività di Ricerca 2022/2024, (ID64)

CRediT authorship contribution statement

Cristiani Lorenzo: Writing – original draft, Conceptualization. **Villano Marianna:** Supervision. **Marandola Clara:** Writing – original draft, Investigation. **Fazi Giuliano:** Investigation. **Zeppilli Marco:** Writing – original draft, Supervision, Conceptualization.

Table 7
Summary of the energetic performance during the 4 experimental periods.

Cathodic material	Graphite granules	Mixed Metal Oxide	Mixed Metal Oxide	Mixed Metal Oxide	Mixed Metal Oxide
Goal	$CO_2 \rightarrow CH_4$	H_2 production	H_2 production + CO_2 abatement GRT 1 h	H_2 production + CO_2 abatement GRT 6 h	CO_2 reduction into CH_4
ΔV (V)	- 1.59 ± 0.25	- 1.63 ± 0.28	- 1.63 ± 0.26	- 1.59 ± 0.25	- 2.49 ± 0.39
CCE (%)	59 ± 4	27 ± 3	58 ± 5	62 ± 5	102 ± 4
ηE (%)	39 ± 3	25 ± 3	53 ± 3	57 ± 3	44 ± 5
EC (kWh/Nm^3CO_2)	0.89 ± 0.08	-	0.62 ± 0.05	1.84 ± 0.13	3.92 ± 0.31
EC_{COD} (kWh/kgCOD)	0.35 ± 0.03	-	0.38 ± 0.04	1.14 ± 0.12	3.24 ± 0.41

Declaration of Competing Interest

The authors declare that they have no known competing financial interests or personal relationships that could have appeared to influence the work reported in this paper.

Data availability

Data will be made available on request.

Acknowledgments

Prof. Mauro Majone is acknowledged for his skillful assistance during each step of this experimentation.

Appendix A. Supporting information

Supplementary data associated with this article can be found in the online version at doi:10.1016/j.bej.2024.109249.

References

[1] P. Weiland, Biogas production: current state and perspectives, Appl. Microbiol. Biotechnol. 85 (4) (2010) 849–860, https://doi.org/10.1007/s00253-009-2246-7.
[2] N. Abatzoglou, S. Boivin, A review of biogas purification processes, Biofuels, Bioprod. Bioref. 3 (1) (2009) 42–71, https://doi.org/10.1002/bbb.117.
[3] I. Angelidaki, L. Treu, P. Tsapekos, G. Luo, S. Campanaro, H. Wenzel, P.G. Kougias, Biogas upgrading and utilization: current status and perspectives, Biotechnol. Adv. 36 (2) (2018) 452–466, https://doi.org/10.1016/j.biotechadv.2018.01.011.
[4] E. Ryckebosch, M. Drouillon, H. Vervaeren, Techniques for transformation of biogas to biomethane, Biomass Bioenergy 35 (5) (2011) 1633–1645, https://doi.org/10.1016/j.biombioe.2011.02.033.
[5] N. Scarlat, J.-F. Dallemand, F. Fahl, Biogas: developments and perspectives in Europe, Renew. Energy 129 (2018) 457–472, https://doi.org/10.1016/j.renene.2018.03.006.
[6] F. Enzmann, D. Holtmann, Rational Scale-Up of a methane producing bioelectrochemical reactor to 50 L pilot scale, Chem. Eng. Sci. 207 (2019) 1148–1158, https://doi.org/10.1016/j.ces.2019.07.051.
[7] F. Enzmann, D. Gronemeier, D. Holtmann, Evaluation of bioelectromethanogenesis part I: energy calculations, Chem. Ing. Tech. 92 (1-2) (2020) 137–143, https://doi.org/10.1002/cite.201900106.
[8] M. Zeppilli, L. Cristiani, E. Dell'Armi, M. Majone, Bioelectromethanogenesis reaction in a tubular microbial electrolysis cell (MEC) for biogas upgrading, Renew. Energy 158 (2020) 23–31, https://doi.org/10.1016/j.renene.2020.05.122.
[9] S. Cheng, D. Xing, D.F. Call, B.E. Logan, Direct biological conversion of electrical current into methane by electromethanogenesis, Environ. Sci. Technol. 43 (10) (2009) 3953–3958.
[10] M. Rosenbaum, F. Aulenta, M. Villano, L.T. Angenent, Cathodes as electron donors for microbial metabolism: which extracellular electron transfer mechanisms are involved? Bioresour. Technol. 102 (1) (2011) 324–333.
[11] L. Cristiani, M. Zeppilli, M. Villano, M. Majone, Role of the organic loading rate and the electrodes' potential control strategy on the performance of a micro pilot tubular microbial electrolysis cell for biogas upgrading, Chem. Eng. J. 426 (2021) 131909, https://doi.org/10.1016/j.cej.2021.131909.
[12] P. Chong, B. Erable, A. Bergel, Microbial anodes: what actually occurs inside pores? Int. J. Hydrog. Energy 44 (9) (2019) 4484–4495, https://doi.org/10.1016/j.ijhydene.2018.09.075.
[13] S. Cheng, B. Logan, Electromethanogenic reactor and processes for methane production, Google Patents, 2013.
[14] W. Zappa, M. Junginger, M. van den Broek, Is a 100% renewable European power system feasible by 2050? Appl. Energy 233-234 (2019) 1027–1050, https://doi.org/10.1016/j.apenergy.2018.08.109.
[15] Europeancommision, REPowerEU Plan, in: E. commision (Ed.) 2022.
[16] R. Sharifian, R.M. Wagterveld, I.A. Digdaya, C. Xiang, D.A. Vermaas, Electrochemical carbon dioxide capture to close the carbon cycle, Energy Environ. Sci. 14 (2) (2021) 781–814, https://doi.org/10.1039/D0EE03382K.
[17] M. Zeppilli, H. Chouchane, L. Scardigno, M. Mahjoubi, M. Gacitua, R. Askri, A. Cherif, M. Majone, Bioelectrochemical vs hydrogenophilic approach for CO2 reduction into methane and acetate, Chem. Eng. J. 396 (2020) 125243, https://doi.org/10.1016/j.cej.2020.125243.
[18] C.M. Dykstra, C. Cheng, S.G. Pavlostathis, Comparison of carbon dioxide with anaerobic digester biogas as a methanogenic biocathode feedstock, Environ. Sci. Technol. 54 (14) (2020) 8949–8957, https://doi.org/10.1021/acs.est.9b07438.
[19] F. Geppert, D. Liu, M. van Eerten-Jansen, E. Weidner, C. Buisman, A. ter Heijne, Bioelectrochemical power-to-gas: state of the art and future perspectives, Trends Biotechnol. 34 (11) (2016) 879–894, https://doi.org/10.1016/j.tibtech.2016.08.010.
[20] M.T. Noori, M.T. Vu, R.B. Ali, B. Min, Recent advances in cathode materials and configurations for upgrading methane in bioelectrochemical systems integrated with anaerobic digestion, Chem. Eng. J. 392 (2020) 123689, https://doi.org/10.1016/j.cej.2019.123689.
[21] H. Xu, K. Wang, D.E. Holmes, Bioelectrochemical removal of carbon dioxide (CO2): an innovative method for biogas upgrading, Bioresour. Technol. 173 (0) (2014) 392–398, https://doi.org/10.1016/j.biortech.2014.09.127.
[22] F. Kong, H.-Y. Ren, D. Liu, Z. Wang, J. Nan, N.-Q. Ren, Q. Fu, Improved decolorization and mineralization of azo dye in an integrated system of anaerobic bioelectrochemical modules and aerobic moving bed biofilm reactor, Bioresour. Technol. 353 (2022) 127147, https://doi.org/10.1016/j.biortech.2022.127147.
[23] G. Lembo, S. Rosa, V. Mazzurco Miritana, A. Marone, G. Massini, M. Fenice, A. Signorini, Thermophilic anaerobic digestion of second cheese whey: microbial community response to H2 addition in a partially immobilized anaerobic hybrid reactor, Processes 9 (1) (2021) 43.
[24] M. Villano, F. Aulenta, C. Ciucci, T. Ferri, A. Giuliano, M. Majone, Bioelectrochemical reduction of CO2 to CH4 via direct and indirect extracellular electron transfer by a hydrogenophilic methanogenic culture, Bioresour. Technol. 101 (9) (2010) 3085–3090, https://doi.org/10.1016/j.biortech.2009.12.077.
[25] M. Zeppilli, M. Simoni, P. Paiano, M. Majone, Two-side cathode microbial electrolysis cell for nutrients recovery and biogas upgrading, Chem. Eng. J. 370 (2019) 466–476, https://doi.org/10.1016/j.cej.2019.03.119.
[26] M. Zeppilli, L. Cristiani, E. Dell'Armi, M. Villano, Potentiostatic vs galvanostatic operation of a microbial electrolysis cell for ammonium recovery and biogas upgrading, Biochem. Eng. J. 167 (2021) 107886, https://doi.org/10.1016/j.bej.2020.107886.
[27] Z. Zhang, Y. Song, S. Zheng, G. Zhen, X. Lu, T. Kobayashi, K. Xu, P. Bakonyi, Electro-conversion of carbon dioxide (CO2) to low-carbon methane by bioelectromethanogenesis process in microbial electrolysis cells: the current status and future perspective, Bioresour. Technol. 279 (2019) 339–349, https://doi.org/10.1016/j.biortech.2019.01.145.
[28] L. Cristiani, M. Zeppilli, C. Porcu, M. Majone, Ammonium recovery and biogas upgrading in a tubular micro-pilot microbial electrolysis cell (MEC), Molecules 25 (2020) 2723.
[29] M. Zeppilli, A. Lai, M. Villano, M. Majone, Anion vs cation exchange membrane strongly affect mechanisms and yield of CO2 fixation in a microbial electrolysis cell, Chem. Eng. J. 304 (2016) 10–19, https://doi.org/10.1016/j.cej.2016.06.020.
[30] M. Zeppilli, P. Paiano, C. Torres, D. Pant, A critical evaluation of the pH split and associated effects in bioelectrochemical processes, Chem. Eng. J. 422 (2021) 130155, https://doi.org/10.1016/j.cej.2021.130155.
[31] L. Cristiani, J. Ferretti, M. Zeppilli, Electron recycle concept in a microbial electrolysis cell for biogas upgrading, Chem. Eng. Technol. 45 (2) (2022) 365–371, https://doi.org/10.1002/ceat.202100534.
[32] Z. Huang, L. Lu, D. Jiang, D. Xing, Z.J. Ren, Electrochemical hythane production for renewable energy storage and biogas upgrading, Appl. Energy 187 (2017) 595–600, https://doi.org/10.1016/j.apenergy.2016.11.099.
[33] C. Cavinato, D. Bolzonella, F. Fatone, A. Giuliano, P. Pavan, Two-phase thermophilic anaerobic digestion process for biohythane production treating biowaste: preliminary results, Water Sci. Technol. 64 (3) (2011) 715–721, https://doi.org/10.2166/wst.2011.698.
[34] W.E. Balch, G.E. Fox, L.J. Magrum, C.R. Woese, R.S. Wolfe, Methanogens: reevaluation of a unique biological group, Microbiol. Rev. 43 (2) (1979) 260–296.
[35] J.G. Zeikus, The biology of methanogenic bacteria, Bacteriol. Rev. 41 (2) (1977) 514–541.
[36] G. Mancini, A. Luciano, D. Bolzonella, F. Fatone, P. Viotti, D. Fino, A water-waste-energy nexus approach to bridge the sustainability gap in landfill-based waste

management regions, Renew. Sustain. Energy Rev. 137 (2021) 110441, https://doi.org/10.1016/j.rser.2020.110441.
[37] T.H.J.A. Sleutels, H.V.M. Hamelers, R.A. Rozendal, C.J.N. Buisman, Ion transport resistance in microbial electrolysis cells with anion and cation exchange membranes, Int. J. Hydrog. Energy 34 (9) (2009) 3612–3620, https://doi.org/10.1016/j.ijhydene.2009.03.004.
[38] M. Tucci, D. Fernández-Verdejo, M. Resitano, P. Ciacia, A. Guisasola, P. Blánquez, E. Marco-Urrea, C. Cruz Viggi, B. Matturro, S. Crognale, F. Aulenta, Toluene-driven anaerobic biodegradation of chloroform in a continuous-flow bioelectrochemical reactor, Chemosphere 338 (2023) 139467, https://doi.org/10.1016/j.chemosphere.2023.139467.
[39] G. Gahleitner, Hydrogen from renewable electricity: an international review of power-to-gas pilot plants for stationary applications, Int. J. Hydrog. Energy 38 (5) (2013) 2039–2061, https://doi.org/10.1016/j.ijhydene.2012.12.010.
[40] M. Zeppilli, E. Dell'Armi, L. Cristiani, M. Petrangeli Papini, M. Majone, Reductive/oxidative sequential bioelectrochemical process for perchloroethylene removal, Water 11 (12) (2019) 2579.
[41] T.-L. Chen, L.-H. Chen, Y.J. Lin, C.-P. Yu, H.-w Ma, P.-C. Chiang, Advanced ammonia nitrogen removal and recovery technology using electrokinetic and stripping process towards a sustainable nitrogen cycle: a review, J. Clean. Prod. 309 (2021) 127369, https://doi.org/10.1016/j.jclepro.2021.127369.
[42] J. Liebetrau, N. Rensberg, D. Maguire, D. Archer, D. Wall, J.D. MurphyRenewable Gas – discussion on the state of the industry and its future in a decarbonised world, Murphy, J.D. (Ed.) IEA Bioenergy Task 37, 11. 2021.
[43] Jd Hullu, J.I.W. Waassen, P.A. Van Meel, S. Shazad, J.M.P. Vaessen, Comparing Different Biogas Upgrading Techniques, Eindhoven University of Technology,, 2008, p. 56.